SLAC-PUB-9681
LCLS-TN-03-1
March 2003

6D Phase Space Measurements at the SLAC Gun Test Facility*

J.F. Schmerge, P.R. Bolton, J.E. Clendenin, D.H. Dowell,
S.M. Gierman, C.G. Limborg and B.F. Murphy

Stanford Linear Accelerator Center
2575 Sand Hill Rd,
Menlo Park, CA 94025, USA
E-mail: Schmerge@slac.stanford.edu

Proposed fourth generation light sources using SASE FELs to generate short pulse, coherent X-rays require demonstration of high brightness electron sources. The Gun Test Facility (GTF) at SLAC was built to test high brightness sources for the proposed Linac Coherent Light Source at SLAC. The GTF is composed of an S-band photocathode rf gun with a Cu cathode, emittance compensating solenoid, single 3 m SLAC linac section and e-beam diagnostic section with a UV drive laser system. The longitudinal emittance exiting the gun has been determined by measuring the energy spectrum downstream of the linac as a function of the linac phase. The e-beam pulse width, correlated and uncorrelated energy spread at the linac entrance have been fit to the measured energy spectra using a least square error fitting routine. The fit yields a pulse width of 2.9 ps FWHM for a 4.3 ps FWHM laser pulse width and 2% rms correlated energy spread with 0.07% rms uncorrelated energy spread. The correlated energy spread is enhanced in the linac to allow slice emittance measurements by conducting a quadrupole scan in a dispersive section. The normalized slice emittance has been measured to be as low as 2 mm-mrad for beams with peak currents up to 150 A (300 pC with a laser pulse length of 1.8 ps) while the full projected emittance is 3 mm-mrad.

1. Introduction

High brightness electron beams are required to drive future 4th generation light sources and as injectors for linear colliders or future laser driven accelerators. A 4th generation light source called the Linac Coherent Light Source (LCLS) has been proposed at SLAC [1]. The LCLS is a SASE FEL at 1.5 Å wavelength which necessarily requires a small transverse and longitudinal emittance electron beam. To reach saturation in a 100 m long undulator, the current design of the LCLS requires an injector capable of producing a bunch with 1 nC of charge, transverse emittance of < 1 mm-mrad, energy spread of < 0.1 % and pulse length of 10 ps. The SLAC Gun Test Facility (GTF) was built to demonstrate the necessary emittance for the LCLS.

*Work supported in part by the Department of Energy under contract number DE-AC03-76SF00515
Presented at the Joint ICFA Advanced Accelerator and Beam Dynamics Workshop:
The Physics and Applications of High Brightness Electron Beams,
7/1/2002 - 7/6/2002, Chia Laguna, Sardinia, Italy

The GTF consists of a Nd:glass drive laser, 1.6 cell S-band rf gun, emittance compensating solenoid, 3 m SLAC linac and diagnostic section. The diagnostics include a quadrupole doublet, multiple beam profile screens and a spectrometer magnet [2]. Figure 1 shows a schematic representation of the GTF also showing the phosphor screen installed downstream of the spectrometer magnet which is used to measure the energy spectra and beam sizes reported here.

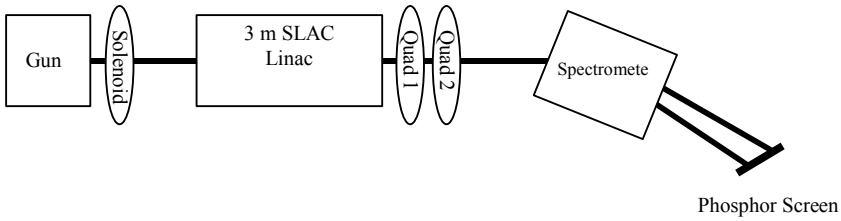

Figure 1. A simplified schematic of the GTF accelerator is shown including the gun, solenoid, linac, quadrupole doublet, spectrometer magnet and phosphor screen used to measure the beam sizes. Quad 1 focuses in the dispersive plane and Quad 2 in the non-dispersive plane.

Previously we have reported projected transverse emittance measurements of 1.5 mm-mrad with 200 pC of charge and a 2 ps FWHM laser pulse [3]. In this paper we describe the longitudinal emittance measurements and transverse slice emittance measurements technique using a linearly chirped electron bunch. The laser pulse lengths used in the experiments are Gaussian shaped with either 1.8 ps or 4.3 ps FWHM pulse length [3]. The UV pulse length was measured with a DRS Hadland FS300 streak camera with reported UV resolution of < 1 ps. The longitudinal emittance measurements are conducted by measuring the beam size on the spectrometer screen in a dispersive section as a function of the linac phase. The slice emittance measurements are obtained by performing a quadrupole scan on a linearly chirped electron beam using the same screen. Both techniques are described in greater detail in the next section.

2. Longitudinal Phase Space

2.1. *Measurement Technique*

The longitudinal emittance of the beam entering the linac is determined by measuring the energy spectrum downstream of the linac as a function of the linac phase. The longitudinal distribution can be described by three parameters - pulse width, correlated energy spread and uncorrelated energy spread - analogous to the three independent beam matrix parameters in transverse phase space. However, space charge and the sinusoidal dependence of the applied RF field tend to distort the longitudinal emittance ellipses so that it is necessary to introduce two additional parameters to fully characterize

the longitudinal emittance exiting the RF gun [4]. The energy spread of the beam, ΔE, is given by Equation (1.1) as a function of the deviation from the centroid temporal position, Δt. Here τ_{11} is the square of the pulse length, τ_{22} is the square of the energy spread, and τ_{12} is related to the ellipse tilt angle. The emittance is defined as the ellipse area divided by π or in terms of the beam matrix as $\varepsilon_l^2 = \tau_{11}\,\tau_{22} - \tau_{12}^2$. The coefficients a and b are the quadratic and cubic perturbation terms added to account for the RF field and space charge forces respectively.

$$\Delta E = \pm\sqrt{\left(\frac{\tau_{12}}{\tau_{11}}\Delta t\right)^2 - \frac{\tau_{22}\Delta t^2 - \varepsilon_l^2}{\tau_{11}}} + \frac{\tau_{12}}{\tau_{11}}\Delta t + a\Delta t^2 + b\Delta t^3 \qquad (1.1)$$

The initial longitudinal beam distribution given by Equation (1.1) is mapped through the linac for each time slice using the linac energy gain equation shown in Equation (1.2) where E_t is the total energy after the linac, E_g is the energy of the particle exiting the gun, E_l is the peak energy gain through the linac and θ_l is the particle phase in the linac.

$$E_t = E_g + E_l\cos(\theta_l) \qquad (1.2)$$

It is assumed that all particles travel at the speed of light, and no wakefields in the linac are included in this calculation. After populating an initial distribution with up to 200,000 particles one can calculate the expected distribution at the linac exit according to the equation above and compare with the measured spectra. Using a least square error routine to minimize the error between the fit and measured value one can estimate the longitudinal emittance. Thus the measurement technique is very similar to the quad scan technique used to measure the transverse emittance except the data is fit to the entire spectrum because of the nonlinear phase space distortions instead of just the rms energy spread.

For the data reported here, energy spectra were recorded at ten different linac phases including the phase corresponding to the minimum energy spread and the maximum energy which is by definition 0° phase. The energy spectra were measured using a Pulnix TM7EX camera imaging the spectrometer phosphor screen, which is mounted at 45° with respect to the bend plane. The integrated spectrometer field along the curved beam trajectory was measured prior to installation for the absolute energy measurement. The spectrometer was calibrated to be 1.9 keV/pixel by varying the spectrometer current and measuring the resulting beam motion on the screen. The resolution of the spectrometer is estimated to be approximately 3-5 keV rms limited by the finite beam spot size at the input plane.

2.2. *Results*

Five spectra were captured at each phase setting along with a single background image with the laser off. The absolute phase was determined experimentally by varying the phase until the maximum energy was found and defining this phase as 0°. The minimum energy spread (0.1% FWHM) occurs at a phase of –13°. The energy spread was measured at 10 different phases in 5° steps on both sides of the minimum. The spectra were background subtracted and averaged over the five images.

The laser pulse length was set at 4.3 ps FWHM, with 38° injection phase with respect to the zero field and the gun was operated at a 110 MV/m gradient. The average energy of the particles exiting the gun is 5.8 MeV, the linac gradient was set at E_l = 25 MeV and the bunch charge is approximately 150 pC. The solenoid field was operated at 2 kG to produce a waist near the spectrometer input plane so no other focusing elements were required. The five independent parameters in Equation (1.1) were varied to best fit the measured energy spectra with a least square error fitting routine and the results are reported in Table 1.

Table 1. The values of the fit parameters from Equation (1.1) using a least square error fitting routine. The parameters are fit at the linac entrance.

parameter	value	units
τ_{11}	1.5	ps^2
τ_{12}	-150	keV ps
τ_{22}	14000	keV^2
ε_l	4.6	keV ps
a	4.0	keV/ps^2
b	3.0	keV/ps^3

Figure 2 shows four of the measured spectra at the indicated linac phase along with the corresponding fits at the linac exit. The fit yields an e-beam pulse length of 1.2 ps rms (2.9 ps FWHM) with 2% rms energy spread (8% FWHM) at the linac entrance. The uncorrelated energy spread was computed to be 3.7 keV rms (.067%) by eliminating all correlations in the distribution and computing the remaining rms energy spread. The measured uncorrelated energy spread and longitudinal emittance is limited by the spectrometer's resolution since the resolution is estimated at 3-5 keV. The finite resolution of the spectrometer is not included in the analysis and accounts for the difference between the fit and the measurement for the lowest energy spread case shown in Figure 2.

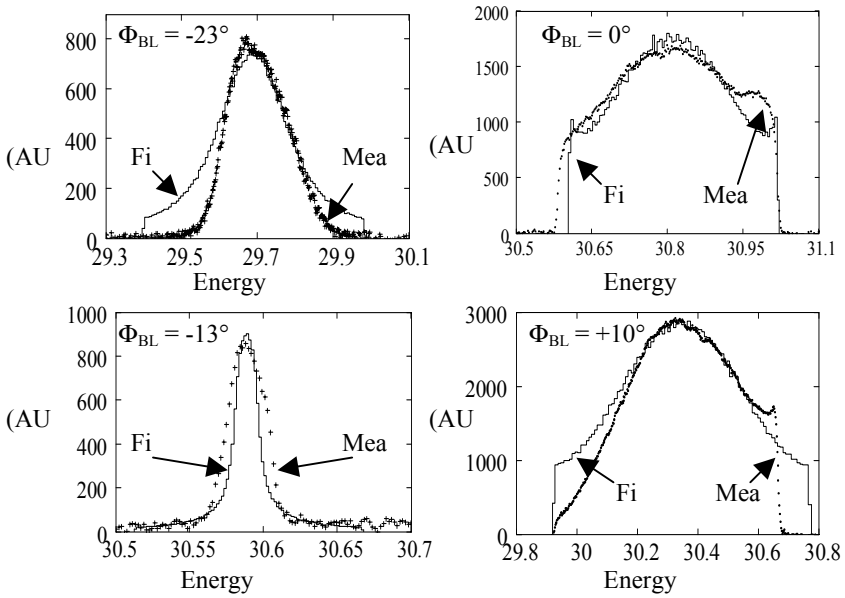

Figure 2. The measured energy spectra and fits in arbitrary units vs energy are shown for four different linac phases. The maximum energy occurs by definition at 0° and the minimum energy spread occurs at a linac phase of -13°.

Figure 3 shows the computed longitudinal distribution at the linac entrance as well as the linac exit for both the minimum energy spread and maximum energy cases. It can be seen that the energy spread at the linac entrance is dominated by the linear chirp while at the linac exit it is strongly dependent on the linac phase. The minimum energy spread occurs at the phase, which nearly removes the linear term and only leaves higher order correlation terms plus the uncorrelated energy spread. At the linac entrance, the additional correlated energy due to the quadratic and cubic terms is 6.1 keV and 5.6 keV respectively for the rms pulse length of $\Delta t = 1.2$ ps. The strong presence of the cubic term in Figure 3 indicates that space charge has a significant effect on the longitudinal phase space despite the modest 50 A peak current.

The measured values are consistent with PARMELA simulations except for the correlated energy spread. PARMELA only predicts an energy spread of approximately 1-2 % FWHM instead of the measured 8%. While this discrepancy is not yet completely understood, it may be partially due to the fact that longitudinal wakefields are not included in PARMELA. However, analytic calculations of the energy spread contribution due to the wakefield in the gun and linac predict energy spreads an order of magnitude less than the measurement. Alternatively, a large correlated energy spread from the gun can be produced if the ratio of the field in the two cells of the gun is not sufficiently close to unity. The gun fields are currently being measured using a bead drop technique and new calibrated probes installed so that the field can be measured at high power in both cells simultaneously to determine if a

dynamic imbalance occurs due to rf heating and subsequent thermal distortions.

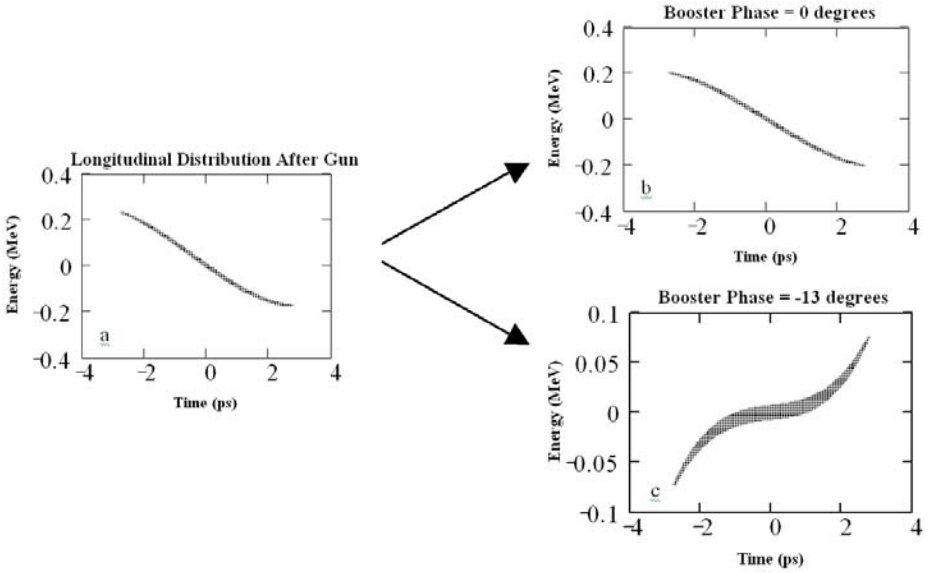

Figure 3. The computed longitudinal phase space at the linac entrance (a), the linac exit with a phase of 0° (b) and the linac exit with a phase of -13° (c). The linac phase can be adjusted to nearly remove the linear chirp resulting in the phase space shown in (c) with a dominant nonlinear term.

Finally phase slippage in the linac is not included in the analysis reported here. However, calculations of the energy spread due to slippage for parameters used in this experiment do not significantly alter the results since the bunch length is short and therefore all particles slip by nearly the same amount. Likewise almost no ballistic bunching or anti-bunching occurs in the linac.

3. Transverse Emittance Measurement

3.1. *Slice Emittance Measurement Technique*

The projected emittance is defined as the emittance of the beam including all the particles in the bunch regardless of longitudinal position while slice emittance is defined as the emittance of the particles from a particular longitudinal or temporal slice of the beam. Typical emittance measurements report only the projected emittance although simulations consistently show the emittance to be a function of longitudinal position. Assuming a time-energy correlation can be introduced into the beam, the emittance can be measured as a function of time in a dispersive section using a quadrupole scan or other emittance measurement technique [5-6]. The slice emittance measurements yield significantly more information than projected emittance alone. As mentioned in the previous section the time energy correlation already exists in the beam at the linac entrance and can also be present in the beam exiting the linac depending on the linac phase. To measure the slice emittance we enhanced the energy chirp exiting the gun by

operating the linac at a phase of +5°. For this experiment the beam size is measured on the phosphor screen in the dispersive section, shown in Figure 1, as a function of quadrupole strength. The beam size in the non-dispersive plane is measured for 10 different temporal or energy slices instead of measuring the temporal or energy distribution as in the previous section. The complete chirped beam profile is acquired in a single shot and then sliced via software for analysis. In addition the software can also integrate in the time or energy axis to yield a projected emittance for comparison with the slice emittances. The longitudinal emittance measurement described in the previous section can be used to calibrate the temporal axis.

In addition to the quadrupole focusing elements in the GTF beamline, the focusing properties of the spectrometer magnet must also be included in the slice emittance analysis. Beam-based techniques were used to determine the spectrometer pole face rotations. This was necessary since the spectrometer was not fully characterized before installation. Subsequent magnetic measurements performed after the electron beam measurements were completed, resulted in almost no change in the computed emittances.

The number of slices that can be resolved is limited to the resolution of the energy or time measurement. Therefore the resolution depends on the minimum spot size that can be obtained at the spectrometer screen and the uncorrelated energy spread. For the GTF parameters, simulations show that the dispersive plane beta function can be kept approximately constant at 5 cm while the quadrupole scan varies the non-dispersive plane beta function from 1-10 m assuming identical Twiss parameters in the two planes at the entrance to the first quadrupole. Thus for a 30 MeV beam the beam size in the dispersive plane is less than 100 μm rms which is equivalent to approximately 2 pixels. For the uncorrelated energy spread reported in the previous section the rms width is also approximately 2 pixels. For the data reported below each of the ten slices is integrated over approximately 30 pixels. Thus the measurement is far from the resolution limit.

3.2. *Results*

The laser used for the slice emittance measurements was approximately 2 ps FWHM in the longitudinal dimension and nearly flat in the transverse dimension due to a clipping aperture. The beam charge was 300 pC and the gun field was 110 MV/m with an injection phase of approximately 30°. The linac was operated at approximately 8 MV/m and +5° phase resulting in the measured total energy of 30 MeV.

Beam size measurements were made at three different solenoid settings and between 13 and 18 different quadrupole strengths for each solenoid setting. Five beam images are obtained at each quadrupole setting and an image with no laser beam incident on the cathode is used for background subtraction. The rms beam sizes are calculated after fully projecting each slice in the dispersive plane and then truncating the wings at 5% of the peak value to minimize the effect in the data analysis of non-beam-related pixels. The beam profile for each slice of a typical image is shown in Figure 4.

The average of the five beam widths are then used to fit the Twiss parameters. Figure 5 shows the normalized emittance, alpha and beta functions as a function of slice number for all three solenoid settings where slice 0 is defined as the full projected value of all ten slices. The phase space mismatch parameter is also plotted in Figure 5, which quantifies the relative misalignment between phase space ellipses. The mismatch parameter [7], ζ, is defined in Equation (1.3) where α_n, β_n and γ_n are the n^{th} slice Twiss parameters while α_0, β_0 and γ_0 are the projected Twiss parameters. A mismatch parameter of 1 means perfect alignment and should be less than 2 for good phase space matching.

$$\zeta_n = \frac{1}{2}\left(\gamma_n\beta_0 - 2\alpha_n\alpha_0 + \gamma_0\beta_n\right) \geq 1 \tag{1.3}$$

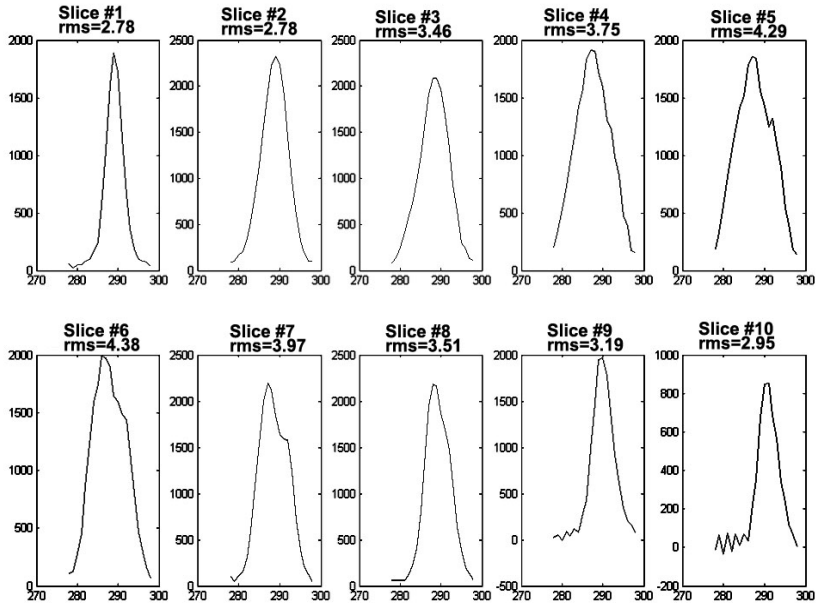

Figure 4. The slice beam projections are shown as a function of pixels. The calibration is 42 μm/pixel and the head of the bunch is slice # 1 and the tail is slice # 10. The rms width of each slice in pixels is reported above each projection.

Typically the head and tail data points should be ignored because the data is dominated by noise due to the small number of particles in these extreme slices. The minimum measured projected emittance is 3 mm-mrad while the minimum slice emittance is approximately 2 mm-mrad. However, the actual emittance minimum was probably not observed in this data set as the emittance is still decreasing as the solenoid decreases. Interestingly the slice emittances depend on the solenoid value. This may be due to centroid offsets between slices and will be investigated further.

The temporal axis for this data set was not calibrated although in principal it can be calibrated with the longitudinal emittance measurement. The calibration is estimated to be approximately 200 fs/slice since there are 10 slices and the laser pulse length was 2 ps FWHM. We have found this technique very powerful in discovering and removing longitudinal correlations in the transverse profile such as those due to wakefields and misalignments. The primary limitation of the technique is that the linac phase can not be varied as it must be properly set to chirp the electron beam.

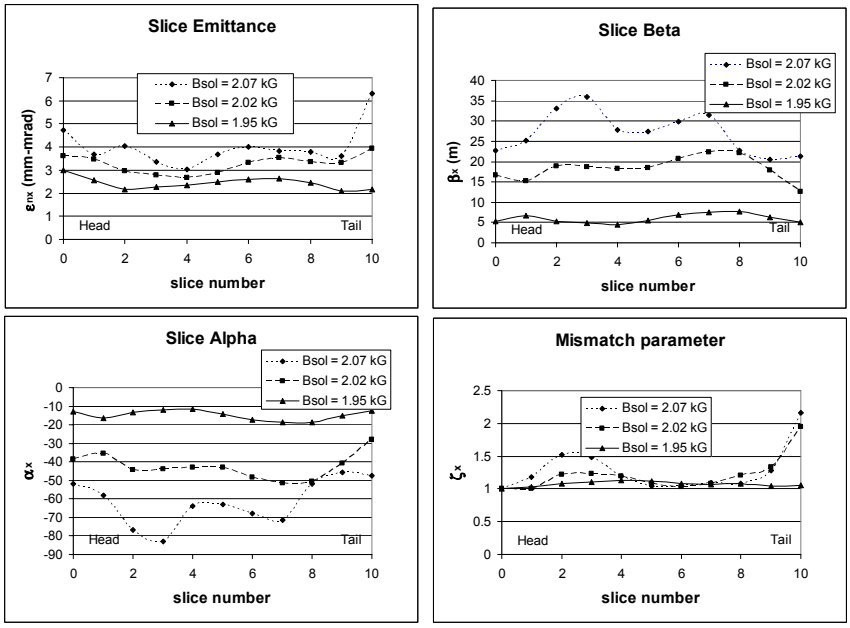

Figure 5. The Twiss parameters including normalized emittance and the mismatch parameter are plotted as a function of slice number for three different solenoid values. Slice 0 is the full projected value while slice 1 is the head and 10 is the tail.

4. Conclusions

We have shown results from a longitudinal emittance measurement using a phase scan technique, which includes nonlinear terms in the fit. The results show a linear correlated energy spread of 8% FWHM between the gun

and linac. The cause of this energy spread has not yet been determined. We are planning further experiments to discover the source of the correlated energy spread and eliminate it in order to improve the beam quality.

In addition we have demonstrated a slice emittance measurement technique by utilizing a quadrupole scan with a chirped electron beam in a dispersive section. This technique allows for quick measurement of the slice emittance since it requires no more time than a normal quadrupole scan measuring the projected emittance. The slice Twiss parameters yield much more information than a simple projected measurement since it reveals the presence of correlations along the bunch. Likewise it provides the possibility for further improvements of the electron beam quality by optimizing the accelerator parameters to remove the correlations. To date we have measured slice emittances of 2 mm-mrad in a slice with peak current estimated at 150 A with 300 pc charge per bunch. We have also observed that the measured slice emittance varies with solenoid field.

Acknowledgments

The Authors would like to thank D. Palmer from SLAC and J. Rosenzweig from UCLA for the loan of the single crystal copper cathode used in the experiment. We would also like to acknowledge L. Serafini for interesting discussions about slice emittance and phase space alignment and W. Graves for help with the slice emittance experiments. Finally we appreciate the assistance of A. Mueller with the graphics.

References

1. See the LCLS home page at http://www-ssrl.slac.stanford.edu/lcls/
2. J.F. Schmerge, M. Hernandez, M.J. Hogan, D.A. Reis, and H. Winick, *in SPIE* **3614**, 22 (1999).
3. J.F. Schmerge, P.R. Bolton, J.E. Clendenin, F.-J. Decker, D.H. Dowell, S.M. Gierman, C.G. Limborg, and B.F, Murphy, *Nucl. Instr. Meth. A* **483**, 301 (2002).
4. D.H. Dowell, S. Joly, A. Loulergue, J.P. deBrion and G. Haouat, *Physics of Plasmas* **4,** 3369 (1997).
5. C.Limborg, P.Bolton, J.Clendenin, D.Dowell, P.Emma, S.Gierman, B.Murphy, J.Schmerge, "PARMELA vs Measurements for GTF and DUVFEL" *Submitted to EPAC 2002*, Paris, June (2002).
6. W.Graves et al. "Experimental study of sub-ps slice electron beam parameters in a photoinjector" *Submitted to Phys. Rev. ST-AB*, (2002).
7. D.A. Edwards and M.J. Syphers, *An Introduction to the Physics of High Energy Accelerators* Wiley, p. 237, (1993).